

ARTICLE

Bridging population pharmacokinetic and semimechanistic absorption modeling of APX3330

Larissa L. Silva¹  | Robert E. Stratford¹  | Richard Messmann²  |
Mark R. Kelley^{3,4,5}  | Sara K. Quinney^{1,5,6,7} 

¹Division of Clinical Pharmacology, Department of Medicine, Indiana University School of Medicine, Indiana, Indianapolis, USA

²Apexian Pharmaceuticals, Indianapolis, Indiana, USA

³Departments of Biochemistry and Molecular Biology, and Pharmacology and Toxicology, Indiana University School of Medicine, Indianapolis, Indiana, USA

⁴Department of Pediatrics, Herman B Wells Center for Pediatric Research, Indiana University School of Medicine, Indianapolis, Indiana, USA

⁵Indiana University Simon Comprehensive Cancer Center, Indiana University School of Medicine, Indianapolis, Indiana, USA

⁶Department of Obstetrics and Gynecology, Indiana University School of Medicine, Indianapolis, Indiana, USA

⁷Center for Computational Biology and Bioinformatics, Indiana University School of Medicine, Indianapolis, Indiana, USA

Correspondence

Sara K. Quinney, 950 W. Walnut St., R2 476, Indianapolis, IN 46202, USA.
Email: squinney@iu.edu

Funding information

National Institute of Health, Grant/Award Number: R01HL140961 and R01EY031939; National Cancer

Abstract

APX3330 ((2E)-2-[(4,5-dimethoxy-2-methyl-3,6-dioxo-1,4-cyclohexadien-1-yl)methylene]-undecanoic acid), a selective inhibitor of APE1/Ref-1, has been investigated in treatment of hepatitis, cancer, diabetic retinopathy, and macular edema. APX3330 is administered orally as a quinone but is rapidly converted to the hydroquinone form. This study describes the pharmacokinetics of APX3330 and explores effect of food on absorption. Total plasma quinone concentrations of APX3330 were obtained following oral administration from studies in healthy Japanese male subjects (single dose-escalation; multiple-dose; food-effect) and patients with cancer patients. Nonlinear mixed effects modeling was performed using Monolix to estimate pharmacokinetic parameters and assess covariate effects. To further evaluate the effect of food on absorption, a semi-physiologic pharmacokinetic model was developed in Gastroplus to delineate effects of food on dissolution and absorption. A two-compartment, first order absorption model with lag time best described plasma concentration-time profiles from 49 healthy Japanese males. Weight was positively correlated with apparent clearance (CL/F) and volume. Administration with food led to an 80% higher lag time. CL/F was 41% higher in the cancer population. The semi-physiologic model indicates a switch from dissolution-rate control of absorption in the fasted-state to gastric emptying rate determining absorption rate in the fed-state. Oral clearance of APX3330 is higher in patients with cancer than healthy Japanese males, possibly due to reduced serum albumin in patients with cancer. Delayed APX3330 absorption with food may be related to higher conversion to the more soluble but less permeable hydroquinone form in the gastrointestinal tract. Future work should address pharmacokinetic differences between APX3330 quinone and hydroquinone forms.

This work has been presented as a poster/abstract at the 2021 ASCPT Annual Meeting: Silva L, Stratford R, Kelley M, Quinney S. Bridging population pharmacokinetic and physiologically based pharmacokinetic approaches to evaluate APX3330 disposition. American Society for Clinical Pharmacology and Therapeutics Annual Meeting, March, 2021 (virtual). Clinical Pharmacology and Therapeutics 109(S1):PII-019.

This is an open access article under the terms of the [Creative Commons Attribution-NonCommercial-NoDerivs](https://creativecommons.org/licenses/by-nc-nd/4.0/) License, which permits use and distribution in any medium, provided the original work is properly cited, the use is non-commercial and no modifications or adaptations are made.

© 2023 The Authors. *CPT: Pharmacometrics & Systems Pharmacology* published by Wiley Periodicals LLC on behalf of American Society for Clinical Pharmacology and Therapeutics.

Institute, Grant/Award Number:
R01CA254110, R01CA231267,
R01CA205166 and R01CA167291; IU
Simon Comprehensive Cancer Center,
Grant/Award Number: P30CA082709;
Riley Children's Foundation

Study Highlights

WHAT IS THE CURRENT KNOWLEDGE ON THE TOPIC?

APX3330, an APE1/REF-1 inhibitor, has shown promise results in treating hepatitis, cancer, diabetic retinopathy, and diabetic macular edema. APX3330 is administered orally as a quinone but is rapidly converted to its hydroquinone form.

WHAT QUESTION DID THIS STUDY ADDRESS

This study incorporates both population pharmacokinetic and semi-physiologic pharmacokinetic approaches to explore the clinical pharmacokinetics of APX3330.

WHAT DOES THIS STUDY ADD TO OUR KNOWLEDGE?

The clinical pharmacokinetics of APX3330 are described in healthy Japanese men and patients with cancer. Oral clearance was 41% greater in patients with cancer than healthy male volunteers. Variability in oral absorption APX3330 may be dependent on the ratio of the less permeable hydroquinone versus the less soluble quinone form.

HOW MIGHT THIS CHANGE DRUG DISCOVERY, DEVELOPMENT, AND/OR THERAPEUTICS?

We demonstrate the use of semimechanistic modeling to explore potential mechanisms leading to variability of APX3330 absorption identified using population pharmacokinetic approaches.

INTRODUCTION

APX3330 ((2*E*)-2-[(4,5-dimethoxy-2-methyl-3,6-dioxo-1,4-cyclohexadien-1-yl)methylene]-undecanoic acid, formerly called E3330) is a small molecule, first-in-class drug that specifically inhibits APE1/Ref-1 (apurinic/apyrimidinic endonuclease 1/reduction-oxidation (redox) effector factor-1).^{1,2} APE1/Ref-1 has multiple functions including an endonuclease activity active on apurinic/apyrimidinic (AP) sites in DNA in the DNA base excision repair pathway, as well as a role in RNA metabolism. However, a significant additional function of APE1/Ref-1 involves its role in redox signaling and regulating the activation and function of key transcription factors (TFs), such as HIF-1 α , NF κ B, STAT3, AP-1, and others involved in tumor cell growth and metabolism.³⁻⁶

APX3330 increases the unfolding of APE1/Ref-1, leading to a loss of redox signaling activity. This occurs as the cysteine residues in APE1/Ref-1 involved in the redox signaling activity are oxidized preventing the reduction of the target TF, and thereby keeping the TF in an oxidized and inactive state.^{3,5-7}

Following oral administration, APX3330 exhibits high variability in absorption. APX3330 contains a quinoid nucleus, which is also observed in other anticancer compounds.⁸ APX3330 is administered orally as the quinone molecular form, but it is rapidly converted to the hydroquinone form, potentially within the gastrointestinal

(GI) tract. Both forms exhibit extensive hepatic metabolism in vitro via cytochrome P450s and glucuronidation (M. R. Kelley, unpublished data). The redox chemistry of quinones and hydroquinones is closely related to their acid-base chemistry.^{9,10} As the quinone and hydroquinone forms of APX3330 exhibit distinct physiochemical properties (Table 1), presystemic conversion to the hydroquinone may influence absorption. Oral absorption involves a multiple-step and complex process, including drug disintegration, dissolution, permeation, and transport across the GI tract. Absorption can be dependent on physiochemical properties of the drug, formulation, and GI physiology, including gastric emptying, intestinal transit, and intestinal and hepatic metabolism.^{11,12} A variety of modeling and simulation approaches have been developed to improve our understanding and predictive capabilities of the rate and extent of oral drug absorption.¹¹⁻¹⁴

This study aims to describe the clinical pharmacokinetics (PKs) of APX3330, measured as total quinone, in healthy male Japanese volunteers and patients with solid tumors enrolled in a phase I clinical study using a population PK (PopPK) approach. This analysis indicated high variability in oral absorption. Thus, to further understand how the physiochemical differences among the quinone and hydroquinone forms, GI tract physiology, and food may influence APX3330 oral absorption, we utilized a semi-physiologic model incorporating the advanced compartmental absorption and transit (ACAT) model in GastroPlus.

TABLE 1 Physicochemical, biopharmaceutical, and pharmacokinetic disposition properties of APX3330 quinone and hydroquinone forms.

Input parameter	Quinone	Hydroquinone
Physicochemical properties		
Molecular weight (g/mol)	378.47	382.5
pKa (acidic)	5	5
Octanol/water partition coefficients (logP)	4.36	4.03
Polar surface area (\AA^2)	89.9	96.22
Hydrogen bond acceptor	1	3
Biopharmaceutics properties		
Human effective permeability ($\times 10^{-4}$ cm/s)	1.538	0.36
Particle size radius (μm)	25	25
Dose volume (mL)	150	150
pH at reference solubility	4.1	3.55
Solubility at reference pH (mg/mL)	0.034	0.545
Solubility factor	1095.286	105.59
Biopharmaceutics Classification System	Class II	Class I

Absorption

Fasted physiology

C1	0.341
C2	0.735
C3	0.604
C4	2.320
ASF, Stomach	0
ASF, Duodenum	9.93
ASF, Jejunum 1	9.55
ASF, Jejunum 2	9.12
ASF, Ileum 1	8.8
ASF, Ileum 2	8.16
ASF, Ileum 3	7.42
ASF, Cecum	1090.8
ASF, Ascending Colon	2122.8

Fed physiology

C1	0.027
C2	0.188
C3	0.212
C4	0.356
ASF, Stomach	0
ASF, Duodenum	1.16
ASF, Jejunum 1	1.15
ASF, Jejunum 2	1.12
ASF, Ileum 1	1.11

TABLE 1 (Continued)

Input parameter	Quinone	Hydroquinone
ASF, Ileum 2	1.07	
ASF, Ileum 3	1.05	
ASF, Cecum	2.60	
ASF, Ascending colon	3.70	
Distribution and clearance		
Pharmacokinetic model	Two-compartment	
Fraction unbound in plasma	0.15	
Blood/Plasma concentration ratio	0.65	
Liver first-pass extraction (FPE) (%)	11.67	
Clearance (L/h)	0.183	
Volume of distribution – central (L)	3	
k_{12} (1/h)	0.11158	
k_{21} (1/h)	0.0669	

Note: All physicochemical and biopharmaceutical properties were predicted by ADMET Predictor X, except pKa, f_{up} , and P_{eff} , experimental values of the first two were available with Eisai regulatory reports, whereas P_{eff} was calculated using the equation proposed by Winiwarter et al.¹⁷ The default value of particle size radius proposed by GastroPlus was assumed. Biopharmaceutical Classification System based on a dose of 120 mg. C1 to C4 represents coefficients used to calculate the absorption scale factor of each GI tract segment in the ACAT model. k_{12} , central to peripheral compartment transfer constant; k_{21} , peripheral to central compartment transfer constant. Abbreviations: ACAT, advanced compartmental absorption and transit; f_{up} , fraction unbound in plasma; GI, gastrointestinal; P_{eff} , effective permeability; pKa, ionization constant.

METHODS

Plasma concentration data

APX3330 plasma concentration data were obtained from four studies in healthy Japanese male subjects conducted by Eisai: single dose-escalation safety study (10, 30, 60, 120, 180, and 240 mg orally); multiple-dose safety study (120 mg administered once or twice a day orally); food effect single-dose crossover (120 mg oral dose, fasted vs. fed); and a high single-dose safety study of 300, 420, and 600 mg oral doses. Individual-level data were digitized from Eisai clinical trial reports using Engauge Digitizer (<https://github.com/markummittchell/engauge-digitizer/releases>). PK data were also obtained from a study conducted by Apexian, in which APX3330 was administered to patients with cancer at doses ranging from 120 to 360 mg administered twice a day for a total of 22 days. Details of these studies are described in the Appendix S1.

The bioanalytical methods used to quantify APX3330 in both Eisai (high-performance liquid chromatography [HPLC]/UV) and Apexian (HPLC-tandem mass spectrometry) sponsored studies did not discriminate between the quinone and hydroquinone molecular forms. APX3330 quinone form was measured following oxidation of the samples to convert any hydroquinone present to the quinone; thus, measured concentrations represented the total quinone. PopPK and semi-physiologic absorption models were developed based on these total quinone plasma concentrations. See Appendix S1 for additional details of the analytical method.

Population pharmacokinetic analysis

PopPK analysis was performed using a nonlinear mixed effects modeling approach implemented within Monolix 2019 R2 (Lixoft SAS). Structural and variance parameters were estimated using stochastic approximation expectation maximization followed by importance sampling methods. Graphical and statistical evaluation were performed in R 4.0.3¹⁵ and Monolix.¹⁶ Plasma concentrations were fit on a linear scale. No concentrations from the Apexian study were below the lower limit of quantification (LLOQ). Eisai study reports did not specify LLOQ, thus all reported data from the Japanese healthy volunteer study were used in model development.

A staged approach was used to develop the PopPK model. Total quinone APX3330 plasma concentrations in healthy volunteers were first used to develop a PopPK model. Data from the APX3330 study in patients with cancer were then added to that from the healthy volunteer study. Using the final estimates from the model for healthy volunteers as initial estimates, a final model was developed to describe data from both studies. As individuals in the dose-escalation and food-effect studies were studied multiple times, interoccasion variability (IOV) was included in the model.

One- and two-compartment models with first-order elimination from the central compartment and first-order absorption models with and without lag time (t_{lag}) were evaluated. PK parameters, the interindividual variability (IIV) and the inter-occasion variability (IOV) were assumed to be log-normally distributed. An exponential relationship was used to describe both IIV and IOV. Various residual error models, including additive, proportional, and combined were evaluated in the model. A zero-centered mean and normal distribution were assumed for the models' variability. Error models were refined through stepwise elimination of random effects for individual fixed effects to decrease overparameterization. Standard

errors for all parameters were obtained from Monolix. The base structural model was selected based on goodness-of-fit plots, precision of estimates, and Bayesian Information Criteria (BIC).

Identification of possible covariates was based on visual inspection of random effects (Eta) plots. Covariate effects were evaluated for body weight (WT; normalized to 70 kg), dosing occasion or period, dose, and food effect, albumin concentration, and data source (healthy Japanese vs. patients with cancer).

Covariates were incorporated based on a power model, as described by Equation 1 for continuous covariates and Equation 2 for categorical covariates.

$$p_j = p_{\text{pop}} \times \left(\frac{\text{cov}_j}{\widehat{\text{cov}}} \right)^{\beta_{\text{cov}}} \times \exp(\eta_j + \eta_{\text{occ}}) \quad (1)$$

$$p_j = p_{\text{pop}} \times \exp(\beta_{\text{cov}} \times \text{cov}_j) \times \exp(\eta_j + \eta_{\text{occ}}) \quad (2)$$

where p_{pop} is the population typical value, cov_j and $\widehat{\text{cov}}$ represent individual covariate values, and median covariate value for the population, respectively, β_{cov} is the covariate effect coefficient and η_j refers to IIV and η_{occ} to IOV.

Covariates showing evidence of a positive or negative trend in the Eta plots were added individually to the model, and those which reduced the $-2 \log$ -likelihood (-2LL) by at least 3.84 ($p < 0.05$) were maintained. All covariates found significant on univariate analysis were incorporated into the model and were maintained in the final model if their elimination led to an increase in the -2LL of at least 6.63 ($p \text{ value} < 0.01$) upon backward elimination.

Precision of parameter estimates was evaluated by bootstrap analysis, with resampling repeated 1000 times. Parameter estimates obtained from bootstrapping were compared with the final parameter estimates by the population model. The predictive performance was assessed using visual predictive check (VPC) plots in which 250 data sets were simulated using the parameter estimates from the final model. The 50th percentile predicted concentration (median) and the associated 5th and 95th percentile predicted concentrations (90% prediction interval) were plotted and compared with the observed concentrations to ensure that the model could reproduce the data from which it was derived.

Semi-physiologic oral absorption modeling

MedChem Designer 6.0 (Simulation Plus, Inc.) was used to draw the molecular structures of APX3330 quinone and

hydroquinone forms, which were exported to ADMET Predictor X (Simulation Plus, Inc.) to characterize the physicochemical and biopharmaceuticals parameters of each molecular form. The human effective permeability (P_{eff}) was calculated based on polar surface area (PSA), and the number of hydrogen bond donor (HBD) values according to the equation $\log P_{\text{eff}} = 4 - 2.546 - 0.011 \cdot \text{PSA} - 0.278 \cdot \text{HBD}$.¹⁷ The fraction unbound in plasma and ionization constant were described in regulatory reports and used as input, although the provided experimental values did not discriminate between quinone or hydroquinone forms.

The semi-physiologic PK model was developed using GastroPlus 9.8 (Simulation Plus, Inc.). Simulation results were compared with the observed systemic concentration data of APX3330 after oral administration of ascending single doses of 10, 30, 60, 180, 120, 240, 300, 420, and 600 mg of APX3330 hydroquinone in a fasted state, and single or multiple doses of 120 mg in the fed state from the Japanese healthy volunteer studies.

APX3330 quinone is the predominant form absorbed from the GI tract, so the model was developed using the physicochemical properties of the quinone form. Plasma concentration versus time profiles following the 120 mg dose of the APX3330 quinone form were used as training data to develop the ACAT model, as this dose was common across all the studies and conditions (e.g., fasted/fed) evaluated. All other doses were used for model verification purposes. The dosage form selected for all simulations was IR:Tablet (immediate release tablet). Physicochemical and biopharmaceuticals properties were imported from ADMET Predictor X (Table 1). Human fasted or fed physiology model (Table S5) was used, as appropriate, and the optimized logD model (Opt logD Model SA/V 6.1) was applied to calculate the absorption scaling factors (ASFs), a modifier to scale effective surface/volume ratio and other effects influencing absorption for each small intestine compartment (Equation 3) and colon (Equation 4).¹⁸

$$\text{ASF}_{\text{si}} = A \times C2 \times 10^{\left(C1 \frac{\Delta \log D_{\text{pH}-C}}{\Delta \log D_{6.5-C}}\right)} \quad (3)$$

$$\text{ASF}_{\text{colon}} = A \times C3 \times 10^{(C4 \times \log D)} \quad (4)$$

where A represents the surface area-to-volume ratio for each compartment, C is a fitted constant ($C = 6.26$),¹⁸ and $C1$ to $C4$ constants are optimizable constants. We optimized $C1$ to $C4$ using the built-in optimization module within GastroPlus to provide a best fit to observed data.

A full physiologically-based PK (PBPK) distribution model did not adequately describe the plasma

concentration-time curves. Although the volume of distribution for APX3330 predicted using the Lucakova method¹⁹ within the GastroPlus software was similar to the value obtained from PopPK, the shape of the plasma concentration-time curve did not adequately capture the multiple slopes observed in the elimination phase of the clinical data. We were also unable to fit tissue partition coefficients to the available data without incurring model identifiability issues. As the objective of our study was to explore potential mechanisms leading to differences in oral absorption of APX3330, we therefore used a two-compartmental PK model to describe the distribution and clearance of APX3330. Values for intercompartmental rate constants (k_{12} and k_{21}) were optimized based on the PopPK model and estimations provided using the PKPlus module available within GastroPlus.

Population-dependent physiological parameters for 62.4 kg body weight (mean value of Japanese Study population) were obtained using the Population Estimates for Age-Related Physiology module in GastroPlus with a size of 250 virtual subjects, randomly selected by the software. Because we did not develop a full PBPK model, we could not specify race and age for the virtual population.

The performance of the semi-physiologic absorption model was assessed by the mean fold error (MFE – Equation 5) for the PK parameters: area under the curve from time zero to infinity ($\text{AUC}_{0-\infty}$), maximum concentration (C_{max}) and time to reach C_{max} (T_{max}) from each simulation and its correspondent observed data. We also evaluated the average fold error (AFE – Equation 6) of each observed and predicted concentration.

$$\text{MFE} = \frac{\text{PK parameter}_{\text{predicted mean}}}{\text{PK parameter}_{\text{observed mean}}} \quad (5)$$

$$\text{AFE} = 10^{\frac{1}{n} \sum \left| \log \frac{\text{predicted concentration}}{\text{observed concentration}} \right|} \quad (6)$$

The model acceptance criteria included prediction of PK parameters and concentrations within twofold of the corresponding observed values from the single and multiple ascending doses in fasted or fed state studies (MFE and AFE = 0.5–2.0). Graphical and statistical evaluations were generated in R 4.0.3.¹⁵

In order to assess whether APX3330 absorption of a 120 mg dose was controlled by drug permeability or solubility and to better understand the delayed absorption in the presence of a meal, we visually compared the predicted profiles of the amount of APX3330 dissolved and absorbed provided by the ACAT model and computed the differences in time needed by each process (dissolution and absorption) for each physiology (fasted and fed) for both quinone and hydroquinone forms of APX3330.

RESULTS

Population pharmacokinetic analysis

The healthy volunteer study enrolled a total of 49 healthy Japanese male volunteers with mean age of 25.4 years and weighting from 52 to 77 kg. The cancer study included 19 participants: 13 (68.42%) were men, and most identified as White (84.21%) or Hispanic (10.53%). Demographic and anthropometric characteristics are summarized in [Table S3](#). All subjects from the Japanese healthy volunteer cohort were within $\pm 20\%$ of ideal body weight. Patient weights were measured several times (from three to eight occasions) during the phase I cancer trial (predosing, dosing phase, and end of treatment). There was no trend in weight over the course of the study, and the mean weight was 88.3 kg. The combined PopPK model was developed based on 1460 plasma APX3330 concentrations, of which 211 (14.45%) were obtained from the study in patients with cancer.

A two-compartment model with first-order absorption and t_{lag} best described the observed concentration-time course of APX3330 in healthy Japanese volunteers. Inclusion of a t_{lag} provided a clearly superior description of the data (BIC = 5998.53) compared to the model without absorption delay (BIC = 7115.17). Final estimated model parameters are listed in [Table 2](#). The data supported adding IIV on elimination clearance (CL/F), volume of distribution of the central compartment (V_1/F), and k_a , the first order absorption rate constant, and the inclusion of IOV on k_a and t_{lag} . There were covariances among CL/F and V_1/F , and k_a and t_{lag} . The preferred error model was proportional. Both fixed and random effects were precisely estimated, with a relative standard error less than 29%. The goodness-of-fit plots demonstrated an adequate fit ([Figure S1](#)), with observed values versus both population and individual predicted concentrations near the line of identity, without noticeable bias. The individual and populational weighted residuals plots showed a random distribution with no obvious concentration or time-related trends.

For the Japanese healthy volunteer data, visual inspection of covariate plots and likelihood ratio tests showed no period or dose effects on PK parameters. WT was positively correlated with CL/F (Δ -2LL = -14.38) and V_1/F (Δ -2LL = -9.98). We also identified a food effect on t_{lag} (Δ -2LL = -34.06), which explained more than 15% of IOV of this parameter. The administration of APX3330 with food caused a delay in drug absorption, as represented by an 80% higher t_{lag} . Although food was shown to have an effect on k_a during the forward inclusion step, it did not meet the inclusion criteria on backward elimination, and hence is not included as a covariate effect in the final model. The

TABLE 2 Final parameter estimates from population pharmacokinetic analysis of APX3330.

Parameter	Healthy volunteers	Combined data
	Estimate (%RSE)	Estimate (%RSE)
t_{lag} (h)	0.413 (6.01)	0.401 (6.92)
$\beta_{Food,t_{lag}}$	0.746 (16.2)	0.815 (13.5)
k_a (1/h)	0.957 (11.4)	0.894 (9.47)
CL/F (mL/h)	196 (3.01)	193 (2.48)
$\beta_{SubjectSource,CL}$	—	0.409 (13.0)
$\beta_{WT,CL}$	0.8 (24.9)	0.659 (17.6)
V_1/F (mL)	4060 (4.15)	4050 (2.51)
β_{WT,V_1}	0.91 (29.0)	0.839 (12.8)
Q/F (mL/h)	276 (4.46)	276 (4.02)
V_2/F (mL)	4770 (2.13)	4780 (2.00)
Random effects		
ω_{ka}	0.482 (26.0)	0.517 (20.1)
$\omega_{CL/F}$	0.126 (11.2)	0.142 (9.67)
$\omega_{V_1/F}$	0.147 (12.8)	0.141 (12.2)
$\gamma_{t_{lag}}$	0.439 (10.8)	0.515 (9.44)
γ_{ka}	0.626 (12.3)	0.564 (11.5)
Correlations		
CL/F ~ V_1/F	0.537 (22.0)	0.349 (37.0)
t_{lag} ~ k_a	-0.487 (23.5)	-0.476 (26.4)
Residual variability		
Proportional	0.153 (2.28)	0.16 (2.14)

Abbreviations: %RSE, percent relative standard error; CL/F, apparent clearance from central compartment; F, bioavailability; k_a , absorption rate constant; Q/F, apparent inter-compartmental clearance; t_{lag} , lag time; V_1/F , apparent volume of the central compartment; V_2/F , apparent volume of the peripheral compartment; β , covariate effect; γ , inter-occasion variability; ω , inter-individual variability.

effects of significant covariates in each PK parameter are summarized in [Table 2](#).

Addition of the data from patients with cancer to the model resulted in a slightly revised covariate structure and parameter estimates ([Table 2](#), [Figure S2](#)). Visual inspection of Eta versus covariate plots showed a clear difference in CL/F between studies (Japanese healthy volunteers vs. patients with cancer; [Figure 1](#)). Whereas this could be a result of differences in albumin concentrations between participants, other differences in study populations (e.g., age, disease state, and ethnicity) may also contribute to this effect. Thus, the covariate “subject source” was included in the model instead of albumin concentration because it represents a combination of all the differences between the two cohorts. The likelihood ratio test indicated that including this covariate on CL/F resulted in a statistically

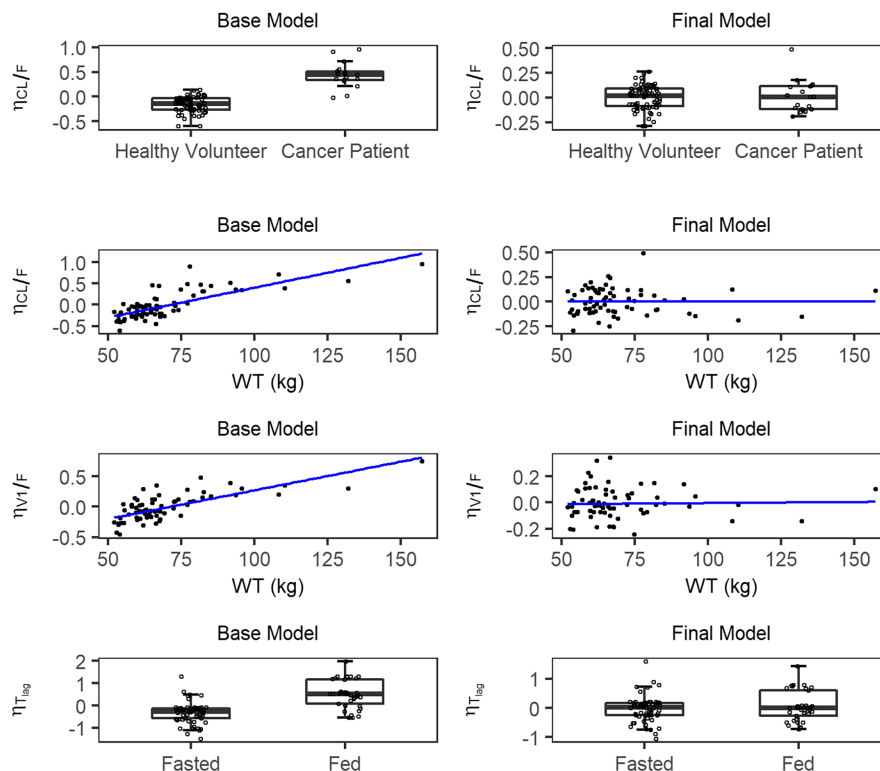


FIGURE 1 Relationship between pharmacokinetic parameters and influential covariates for the base and final model from combined data from Japanese healthy volunteer and patients with cancer. Interindividual variability on CL/F ($\eta_{CL/F}$) versus subject source and versus body weight (kg); inter-individual variability on V_1/F ($\eta_{V1/F}$) versus body weight (kg) and interindividual variability on t_{lag} (η_{Tlag}) versus food, represented by fasted or fed states, are shown. These relationships are illustrated for estimates of η prior to incorporation of covariates effect in the model (left column – base model) or after adjusting for these covariates (right column – final model). The boxes represent the 25th, 50th, and 75th percentiles; the whiskers represent the lowest datum still within 1.5 interquartile ranges (IQRs) of the lower quartile, and the highest datum still within 1.5 IQRs of the upper quartile range; the dots represent observed data, and blue lines represent the result of loess smoother with fitting by weighted least-squares. CL/F , apparent clearance; t_{lag} , time lag; V_1/F , volume of distribution of the central compartment; WT, weight.

improved model fit ($\Delta-2LL = -39.52$). Apparent oral clearance (CL/F) was 41% greater in patients with cancer. The effects of WT on CL/F and V_1/F , as well as food effect on t_{lag} were still significant in the combined data model, as shown in Figure 1.

The VPCs for the combined data model (Figure 2) demonstrated adequate model fit for APX3330 concentrations, with most of the medians and 5th and 95th percentile curves for observed values contained within the corresponding model-predicted confidence regions. Model stability was also evaluated by bootstrapping analysis. The median and 5th and 95th percentiles of estimated parameters from the bootstrap were comparable with the final parameter estimates (Table S4).

Semi-physiologic oral absorption modeling

The biopharmaceutical and physicochemical properties predicted by the ADMET Predictor for APX3330 that were

used as input to GastroPlus to perform all simulations are described in Table 1. Simulated plasma-concentration profiles captured the observed data (Figure S3), with predictions in the range of the 95% confidence interval. Observed and predicted PK parameters AUC, C_{max} , T_{max} met the acceptance criteria, with MFE in the range of 0.74–1.22, 0.83–1.17, and 0.55–1.22, respectively, as summarized in Table 3. The simulated concentrations for the model using fasted physiology presented an AFE of 1.00, whereas for fed physiology, the value was 0.79 (Figure S4).

The IIV in the ratio of quinone to hydroquinone in the GI tract may contribute to high variability in absorption, particularly in the fed state. The hydroquinone form of APX3330 has a higher solubility but lower permeability (P_{eff}) than the quinone form (Table 1). For the quinone form, the similar shape and proximity of the simulated profiles of the amount of APX3330 dissolved in the GI tract and the amount absorbed in the fasted condition (Figure 3) indicated that dissolution largely controlled the rate of APX3330 absorption. The presence of a meal clearly delayed drug absorption,

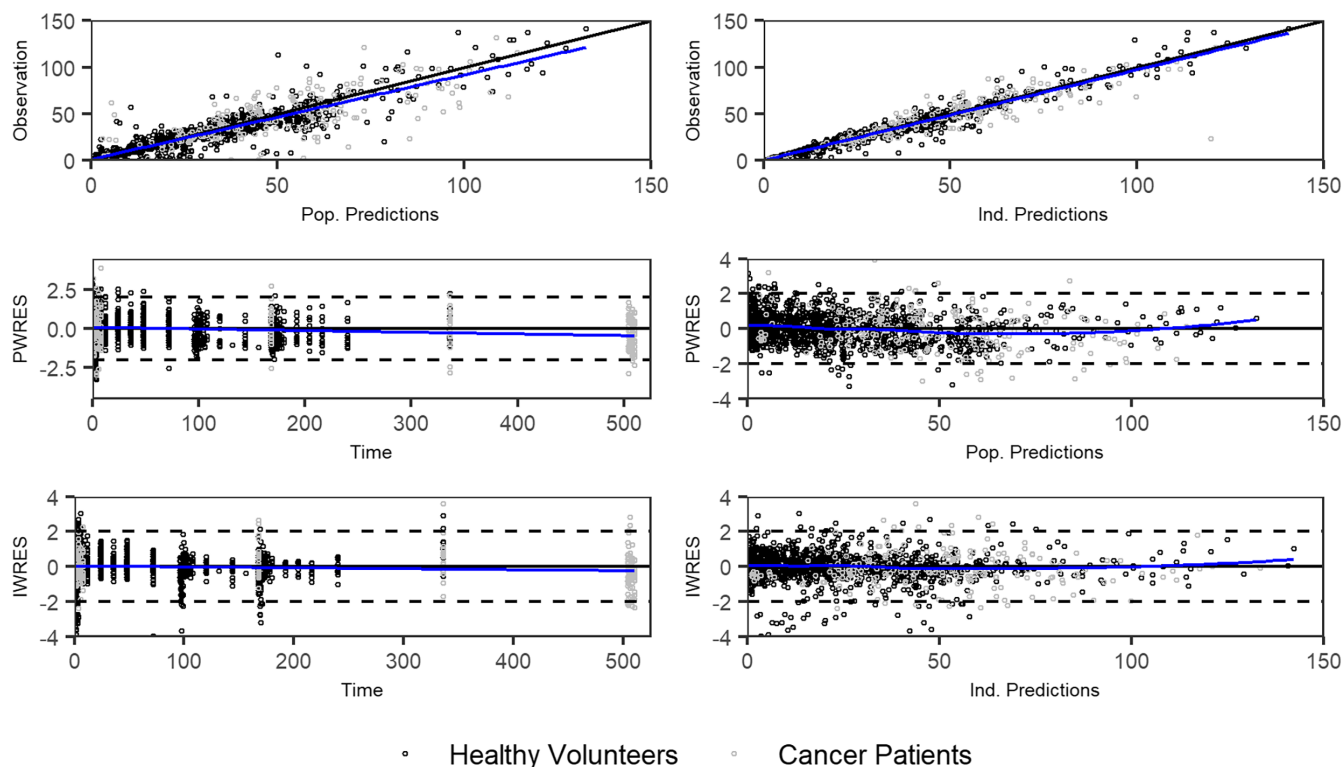


FIGURE 2 Visual predictive checks of APX3330 plasma concentrations including combined data and stratified by single or multiple doses, fasted, or fed state, and subjects' source. The circles represent the observations; the black lines denote the 5th, 50th, and 95th percentiles of the prediction-corrected observed data, the shaded areas denote the confidence interval of the 5th, 50th, and 95th percentiles of the prediction-corrected simulated data. IWRES, individual weighted residuals; PWRES, populational weighted residuals.

with C_{\max} occurring at ~6h in the fed state compared to 2h in the fasted state, which were both described well by the model (Table 3). Predicted time to complete dissolution was increased to 3.3h in the presence of a meal (Figure 3). In addition, there was a substantial shift between predicted dissolution and absorption rate profiles in the fed state, indicating reduced influence of dissolution control on APX3330 absorption in the presence of a meal. In contrast, the hydroquinone undergoes rapid dissolution in both the fed and fasted states. However, food substantially decreases the rate of absorption of the hydroquinone (Figure S5). The differences in permeability between quinone and hydroquinone are more pronounced in the fed state.

DISCUSSION

A PopPK model has been developed to describe the PK properties of APX3330 in a cohort of healthy Japanese volunteers, identifying a food effect on the absorption t_{lag} . Following, the PopPK model was extended to patients with different types of solid tumors. The combined model predicted that patients with cancer have faster elimination than healthy Japanese subjects. The semi-physiologic absorption modeling revealed a change from dissolution

rate control of APX3330 absorption in the fasted state to a different rate-controlling mechanism when administration coincided with a meal.

The final structural PopPK model of APX3330 was a two-compartment model with first-order absorption and t_{lag} . Based on the dose-escalation design in the healthy volunteer study, which involved two groups of six subjects per group receiving three different single-dose levels, we first evaluated period as a covariate, followed by dose administered. Neither period nor dose level were found to be significant, indicating linear PKs over the range of 10–600 mg oral dosing.

Both the PopPK and ACAT modeling approaches identified the effect of food on drug absorption. In the presence of food, the t_{lag} estimated by the PopPK model was 81% higher than in fasted patients. Similarly, the semi-physiologic approach predicted an increase in T_{\max} from 2h under fasted conditions to more than 5h in the fed state. This pattern of delayed absorption is typically observed with high permeability and high solubility drugs (Biopharmaceutics Classification System [BCS] class I),²⁰ where the decrease in the rate of gastric emptying caused by a meal is the primary mechanism involved.^{11,21}

Despite the small IIV for CL/F and V_1/F estimates, inclusion of WT as a covariate significantly improved the

	Trial (dose, physiology)	AUC ($\mu\text{g mL/h}$)	C_{max} ($\mu\text{g/mL}$)	T_{max} (h)
Observed	10 mg, fasted	52.2	2.08	2.0
Predicted		48.1	2.29	1.5
MFE		0.93	1.10	0.77
Observed	30 mg, fasted	166	6.41	3.0
Predicted		144	6.87	1.6
MFE		0.87	1.07	0.55
Observed	60 mg, fasted	333	13.1	2.0
Predicted		289	13.4	1.6
MFE		0.87	1.05	0.82
Observed	120 mg, fasted ^a	690	28.0	2.0
Predicted		578	27.4	1.6
MFE		1.19	1.02	1.22
Observed	120 mg, fed ^a	753	24.5	6.0
Predicted		576	20.4	5.5
MFE		0.77	0.83	0.91
Observed	120 mg q.d., fed	688	44.6	5.1
Predicted		564	34.3	5.0
MFE		1.22	0.77	1.0
Observed	120 mg b.i.d., fed	593	52.0	5.0
Predicted		558	53.3	5.0
MFE		1.06	1.03	1.0
Observed	180 mg, fasted	987	34.7	3.0
Predicted		868	41.1	1.7
MFE		0.88	1.18	0.56
Observed	240 mg, fasted	1281	46.9	3.0
Predicted		1157	54.8	1.8
MFE		0.90	1.17	0.59
Observed	300 mg, fasted	1839	60.2	3
Predicted		1446	68.2	1.9
MFE		0.79	1.13	0.63
Observed	420 mg, fasted	2728	90.8	3.0
Predicted		2024	95.2	2.0
MFE		0.74	1.05	0.66
Observed	600 mg, fasted	3588	124	2.0
Predicted		2892	135	2.1
MFE		0.81	1.08	1.05

TABLE 3 Mean predicted and observed $\text{AUC}_{0-\infty}$, C_{max} , and T_{max} of APX3330.

Abbreviations: $\text{AUC}_{0-\infty}$, area under the concentration-time curve from 168 to 180 h (b.i.d. dosing) or 192 h (q.d. dosing); C_{max} , peak plasma concentration; MFE, mean fold error; T_{max} , time to reach C_{max} .

^aData used for advanced compartmental absorption and transit (ACAT) model development.

model. When we combined data from healthy volunteer and patients with cancer studies, we observed a significant difference in CL/F between the two data sources, with a 40% higher CL/F in patients with cancer. The higher clearance in this cohort could be reduced plasma protein binding in patients with cancer or differences in

drug metabolizing enzyme activity. Although total albumin levels were within the normal range in both studies,²² they averaged $3.9 \pm 0.28 \text{ g/dL}$ in patients with cancer and $4.8 \pm 0.16 \text{ g/dL}$ in healthy volunteers. As APX3330 is a low extraction drug, hepatic clearance is inversely correlated to protein binding.²³ Although adjusting for serum albumin

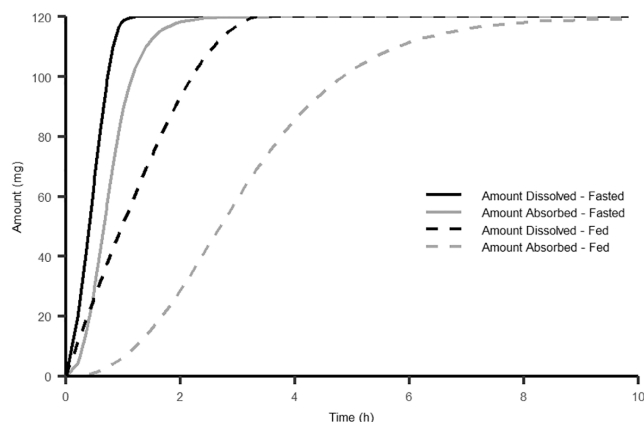


FIGURE 3 Absorption (gray lines) and dissolution (black lines) profile of APX3330 after an oral administration of 120 mg immediate release tablet under fasted (solid lines) and fed (dashed lines) states to a healthy volunteer.

decreased the 2LL by 25.1, a categorical covariate of subject source resulted in a more significant improvement in model fit ($-2LL$ decreased 39.52 from the base model). Because subject source could account for differences between the two study populations in addition to albumin, including disease status (patients with cancer vs. healthy volunteers) and ethnicity of participants, we opted to maintain it in the model instead of albumin concentration.

Although the PopPK model fit the observed data with good agreement, variability in absorption parameters, k_a and t_{lag} , was over 50%. Therefore, the semi-physiologic model was developed to understand better which physicochemical properties of APX3330 quinone and hydroquinone, and GI tract physiology impact the drug absorption process and its interaction with food. The predicted in vivo dissolution and absorption profiles provided by the developed ACAT model showed that dissolution rate, a process influenced by solubility, controls the absorption rate of APX3330 quinone in the fasted state. This would be expected for a BCS class II drug, consistent with the quinone form as predicted by ADMET Predictor X. However, in the presence of a meal, clear evidence of dissolution rate control on absorption rate was not observed. In contrast, the hydroquinone form undergoes rapid dissolution in both fed and fasted states, with its absorption limited by permeability. It appears that absorption of the hydroquinone form is substantially slower than the quinone form and that food further retards its absorption. Therefore, it appears that the ratio of quinone to hydroquinone in the GI tract contributes to the high variability observed in APX3330 absorption.

Food may directly or indirectly impact oral drug absorption, as it can change the GI tract environment, mainly via an increase in gastric pH, as well as prolong gastric residence. Moreover, food-drug interactions depend on drug/formulation properties, dosage regimens,

and food categories (e.g., high-fat meal and high-protein meal).^{11,24} A high-fat meal, which is commonly used in phase I trials conducted in healthy volunteers, can significantly retard gastric emptying and increase the absorption of hydrophobic drugs,^{11,24} such as the quinone form of APX3330. However, the increase in stomach pH observed in the fed state²⁵ could change the rate of interconversion between quinone and hydroquinone forms, as this is pH-dependent.⁹ An increase in this rate, or merely longer time prior to absorption, could have created more of the higher soluble hydroquinone form, which was predicted to be a BCS class I entity. Thus, the meal-induced switch away from dissolution rate control to a permeability rate controlling step in the absorption process or to a gastric emptying control mechanism, which is common for BCS class I drugs, is possibly due to a larger proportion of the hydroquinone form in the fed state. It is essential to understand the mechanisms of food effects because changes in drug absorption can be clinically relevant.²⁴ For APX3330, the extent of absorption remains the same with or without food co-administration, despite its delayed absorption. However, this delay may in turn delay the onset of therapeutic action.¹¹ However, as dosing regimens of APX3330 in both cancer and diabetic retinopathy/Diabetic Macular Edema trials is twice daily (NCT04692688, NCT03375086), any delay in absorption should not be significant with chronic treatment.

There are several limitations to this study. First, as data were extracted from commercially produced study reports, we had limited information on trial design and analytical methods. As different analytical methods were used, this could contribute to the variability observed between studies. Additionally, the analytical methods used were unable to separate the quinone from the hydroquinone moiety of APX3330, hence resulting in total APX3330 plasma concentrations driving model development. Although this limits our ability to verify the PK models, the quinone and hydroquinone moiety of APX3330 exhibit similar potencies and, hence, will not impact the pharmacodynamics of the drug. We were also limited in our ability to develop a full PBPK model due to lack of experimental data to inform parameters and differences between the physicochemical properties of the quinone and hydroquinone form of APX3330. Despite these limitations, we demonstrated that the APX3330 absorption is controlled by its dissolution profile and delayed in the presence of food.

This is the first study to describe the clinical PKs of APX3330. Our approach incorporated both PopPK and semi-physiologic modeling to provide essential insights into the absorption of this drug. These models indicate that the conversion between quinone and hydroquinone moieties within the GI tract, which may be influenced

by the presence of food, could lead to variability in absorption. Although plasma albumin concentration may partially explain the different clearances between the Japanese healthy volunteers and patients with cancer studied, other differences between the study populations may also play a role.

AUTHOR CONTRIBUTIONS

L.S.L., R.E.S., R.M., M.R.K., and S.K.Q. wrote the manuscript. L.S.L., R.E.S., M.R.K., and S.K.Q. designed the research. L.S.L., R.E.S., and S.K.Q. performed the research. L.S.L., R.E.S., and S.K.Q. analyzed the data.

FUNDING INFORMATION

M.R.K. was supported by grants from the National Institute of Health and National Cancer Institute R01CA167291, R01CA205166, R01CA231267, and R01CA254110 and NIH grants R01EY031939 and R01HL140961. M.R.K., R.E.S., and S.K.Q. are supported by the IU Simon Comprehensive Cancer Center, P30CA082709. M.R.K. and S.K.Q. are also supported by the Riley Children's Foundation. L.S.L., R.E.S., and S.K.Q. are also supported by The Indiana University School of Medicine Disease and Therapeutic Response Program which is funded in part by the Indiana Clinical and Translational Sciences Institute award UL1TR002529 from the National Institutes of Health, National Center for Advancing Translational Sciences, Clinical and Translational Sciences Award. The content is solely the responsibility of the authors and does not necessarily represent the official views of the National Institutes of Health or other funders.

CONFLICT OF INTEREST STATEMENT


M.R.K. has licensed APX3330 through Indiana University Research and Technology Corporation to Apexian Pharmaceuticals LLC. R.M. is an employee of Apexian Pharmaceuticals. Apexian Pharmaceuticals had neither control nor oversight of the studies, interpretation, input, or presentation of the data in this manuscript. Apexian Pharmaceuticals has licensed APX3330 to Ocuphire Pharma for clinical trial studies in diabetic retinopathy and diabetic macular edema. M.R.K. is a co-founder of Apexian Pharmaceuticals and is a medical consultant to Ocuphire Pharma who had neither control nor oversight of the studies, input, interpretation, or presentation of the data in this manuscript. All other authors declared no conflicts of interest related to this work.

ORCID

Larissa L. Silva  <https://orcid.org/0000-0002-6165-6893>
Robert E. Stratford  <https://orcid.org/0000-0002-9735-0220>

Richard Messmann  <https://orcid.org/0000-0002-2112-0277>

Mark R. Kelley  <https://orcid.org/0000-0001-9472-1826>

Sara K. Quinney  <https://orcid.org/0000-0002-6554-0695>

REFERENCES

1. Nyland RL, Luo M, Kelley MR, Borch RF. Design and synthesis of novel quinone inhibitors targeted to the redox function of apurinic/aprimidinic endonuclease 1/redox enhancing factor-1 (Ape1/Ref-1). *J Med Chem*. 2010;53:1200-1210.
2. Zou GM, Karikari C, Kabe Y, Handa H, Anders RA, Maitra A. The Ape-1/Ref-1 redox antagonist E3330 inhibits the growth of tumor endothelium and endothelial progenitor cells: therapeutic implications in tumor angiogenesis. *J Cell Physiol*. 2009;219:209-218.
3. Mijit M, Caston R, Gampala S, Fishel ML, Fehrenbacher J, Kelley MR. Ape1/Ref-1 – one target with multiple indications: emerging aspects and new directions. *J Cell Signal*. 2021;2:151-161.
4. Gampala S, Shah F, Lu X, et al. Ref-1 redox activity alters cancer cell metabolism in pancreatic cancer: exploiting this novel finding as a potential target. *J Exp Clin Cancer Res*. 2021;40:251.
5. Gampala S, Shah F, Zhang C, et al. Exploring transcriptional regulators Ref-1 and Stat3 as therapeutic targets in malignant peripheral nerve sheath Tumours. *Br J Cancer*. 2021;124:1566-1580.
6. Caston RA, Gampala S, Armstrong L, Messmann RA, Fishel ML, Kelley MR. The multifunctional Ape1 DNA repair-redox signaling protein as a drug target in human disease. *Drug Discov Today*. 2021;26:218-228.
7. Hartman GD, Lambert-Cheatham NA, Kelley MR, Corson TW. Inhibition of Ape1/Ref-1 for neovascular eye diseases: from biology to therapy. *Int J Mol Sci*. 2021;22:10279.
8. Long DJ, Jaiswal AK. NRH:quinone oxidoreductase2 (NQO2). *Chem Biol Interact*. 2000;129:99-112.
9. Monks TJ, Jones DC. The metabolism and toxicity of quinones, quinonimines, quinone methides, and quinone-thioethers. *Curr Drug Metab*. 2002;3:425-438.
10. Song Y, Buettner GR. Thermodynamic and kinetic considerations for the reaction of semiquinone radicals to form superoxide and hydrogen peroxide. *Free Radic Biol Med*. 2010;49:919-962.
11. Abuhelwa AY, Williams DB, Upton RN, Foster DJ. Food, gastrointestinal pH, and models of oral drug absorption. *Eur J Pharm Biopharm*. 2017;112:234-248.
12. Agoram B, Woltosz WS, Bolger MB. Predicting the impact of physiological and biochemical processes on oral drug bioavailability. *Adv Drug Deliv Rev*. 2001;50:S41-S67.
13. Huang W, Lee SL, Yu LX. Mechanistic approaches to predicting oral drug absorption. *AAPS J*. 2009;11:217-224.
14. Kostewicz ES, Aarons L, Bergstrand M, et al. PBPK models for the prediction of in vivo performance of oral dosage forms. *Eur J Pharm Sci*. 2014;57:300-321.
15. R Core Team. *R: A Language and Environment for Statistical Computing*. R Foundation for Statistical Computing; 2021.
16. Traynard P, Ayral G, Twarogowska M, Chauvin J. Efficient pharmacokinetic modeling workflow with the monolixsuite: a case

- study of remifentanyl. *CPT Pharmacometrics Syst Pharmacol*. 2020;9:198-210.
17. Winiwarter S, Bonham NM, Ax F, Hallberg A, Lennernäs H, Karlén A. Correlation of human jejunal permeability (in vivo) of drugs with experimentally and theoretically derived parameters. A multivariate data analysis approach. *J Med Chem*. 1998;41:4939-4949.
 18. Hens B, Bolger MB. Application of a dynamic fluid and pH model to simulate intraluminal and systemic concentrations of a weak base in gastroplus. *J Pharm Sci*. 2019;108:305-315.
 19. Lukacova V, Parrott N, Lavé T, Fraczekiewicz G, Bolger MB. *General Approach to Calculation of Tissue:Plasma Partition Coefficients for Physiologically Based Pharmacokinetic (PBPK) Modeling*. AAPS National Annual Meeting and Exposition; 2008. <https://www.simulations-plus.com/resource/general-approach-calculation-tissueplasma-partition-coefficients-physiologically-based-pharmacokinetic-pbpb-modeling/>
 20. Amidon GL, Lennernas H, Shah VP, Crison JR. A theoretical basis for a biopharmaceutic drug classification: the correlation of in vitro drug product dissolution and in vivo bioavailability. *Pharm Res*. 1995;12:413-420.
 21. Gu CH, Li H, Levons J, et al. Predicting effect of food on extent of drug absorption based on physicochemical properties. *Pharm Res*. 2007;24:1118-1130.
 22. 5 Human albumin. *Transfus Med Hemother*. 2009;36:399-407.
 23. Benet LZ, Hoener BA. Changes in plasma protein binding have little clinical relevance. *Clin Pharmacol Ther*. 2002;71:115-121.
 24. Deng J, Zhu X, Chen Z, et al. A review of food-drug interactions on oral drug absorption. *Drugs*. 2017;77:1833-1855.
 25. Abuhelwa AY, Foster DJR, Upton RN. A quantitative review and meta-models of the variability and factors affecting oral drug absorption-part I: gastrointestinal pH. *AAPS J*. 2016;18:1309-1321.

SUPPORTING INFORMATION

Additional supporting information can be found online in the Supporting Information section at the end of this article.

How to cite this article: Silva LL, Stratford RE, Messmann R, Kelley MR, Quinney SK. Bridging population pharmacokinetic and semimechanistic absorption modeling of APX3330. *CPT Pharmacometrics Syst Pharmacol*. 2024;13:106-117. doi:[10.1002/psp4.13061](https://doi.org/10.1002/psp4.13061)